www.nature.com/cdd

CDDpress

ARTICLE

Ssu72-HNF4α signaling axis classify the transition from steatohepatitis to hepatocellular carcinoma

Hyun-Soo Kim[1,6]✉, Joon-Sup Yoon[1,6], Yoon Jeon[2], Eun-Ji Park[1], Jin-Kwan Lee[3], Si Chen[1], Ho Lee[2], Jee Young Park[4], Heounjeong Go[5] and Chang-Woo Lee[1,3]✉

Growing evidence suggests a mechanistic link between steatohepatitis and hepatocellular carcinoma (HCC). However, the lack of representative animal models hampers efforts to understand pathophysiological mechanisms underlying steatohepatitis-related HCC. We found that liver-specific deletion of Ssu72 phosphatase in mice, leads to a high incidence of nonalcoholic fatty liver disease and nonalcoholic steatohepatitis, but not HCC. However, loss of Ssu72 drastically increased the probability of HCC developing, as well as the population of hepatic progenitors, in various chemical and metabolic syndrome-induced HCC models. Importantly, hepatic Ssu72 loss resulted in the induction of mature hepatocyte-to-progenitor cell conversion, by dedifferentiation orchestrated by Ssu72-mediated hypo-phosphorylation of hepatocyte nuclear factor 4α (HNF4α), a master regulator of hepatocyte function. Our findings suggest that Ssu72-mediated HNF4α transcription contributes to the progression of steatohepatitis-associated HCC by regulating the dedifferentiation potential of hepatocytes. Thus, targeting the Ssu72-mediated HNF4α signaling that underlies the pathogenesis of steatohepatitis-associated HCC development could be a novel therapeutic intervention for steatohepatitis-associated HCC.

Cell Death & Differentiation (2022) 29:600–613; https://doi.org/10.1038/s41418-021-00877-x

INTRODUCTION

Numerous studies have provided evidence that nonalcoholic fatty liver disease (NAFLD) and nonalcohol steatohepatitis (NASH) are complex and heterogenous diseases regulated by liver parenchymal and non-parenchymal cells [1]. NAFLD ranges from simple steatosis without inflammation, to NASH. It can lead to fibrosis, cirrhosis, and hepatocellular carcinoma (HCC) [1]. Hepatocarcinogenesis is a multistep process in which a number of genetic and epigenetic mutations accumulate in hepatocytes [2, 3]. It includes transition of normal cells through so called tumor initiated cell (TIC), stage to preneoplastic lesions that develop into HCC [4]. However, functional mechanisms that convert terminally differentiated hepatocytes into TICs are poorly understood. During chronic liver damage, hepatocyte regeneration can be observed in the form of progenitor cells [also called facultative stem cells (FSCs) and oval cells in rodents] located around the periportal region (the canals of Hering). These cells have bimodal potential (bipotential). They are capable of proliferation and differentiation into both hepatocytes and cholangiocytes. They typically form a hepatoblast which is comprised of ductules and strings of cholangiocytes in a process termed ductular reaction [5]. Activation of these progenitor cell compartments is associated with an increased risk of HCC development [6]. In contrast, in the early stage of HCC development, hepatocytes are converted into progenitor cells in the pericentral region. Their origin represents a transcriptomic signature similar to the bipotential FSCs that reside within periportal regions [7, 8]. More recently, tumors observed in NASH-associated HCC mouse models have been thought to originate from converted progenitor cells of differentiated pericentral hepatocytes rather than FSCs in the periportal region [9]. Given these circumstances, it is plausible that some bipotential progenitor cells can acquire additional mutations with an associated gain in replicative capacity, thereby facilitating HCC development. NASH with advanced fibrosis is hypocellular and is irreversible [1]. Thus, identifying molecular mechanisms that regulate the progression from hypocellular NASH to NASH-associated HCC could be a substantial breakthrough in understanding NASH-to-HCC conversion.

During liver regeneration after partial liver resection and/or acute liver injury, the proliferative response (also called compensatory proliferation) is necessary for maintenance of liver mass and damage repair. However, hepatocytes do not undergo more than a few rounds of cell division [9, 10]. On the other hand, chronic chemical or high-fat-diet (HFD) interventions can stimulate dedifferentiation of hepatocytes (known to have proliferative potential), which then undergo multiple divisions to give rise to malignant HCC [8]. In the context of HCC development, several groups have shown that terminally differentiated hepatocytes can be transformed into hepatoblasts or biliary cell-like tumors, previously thought to originate exclusively from cholangiocytes

[1]Department of Molecular Cell Biology, Samsung Medical Center, Sungkyunkwan University School of Medicine, Suwon, South Korea. [2]Research Institute, Graduate School of Cancer Science and Policy, National Cancer Center, Goyang, South Korea. [3]Research Institute, Curogen Technology, Suwon, South Korea. [4]Department of Pathology, Kyungpook National University Medical Center, School of Medicine, Kyungpook National University, Daegu, South Korea. [5]Department of Pathology, Asan Medical Center, University of Ulsan College of Medicine, Seoul, South Korea. [6]These authors contributed equally: Hyun-Soo Kim, Joon-Sup Yoon. ✉email: jazz7780@skku.edu; cwlee1234@skku.edu

Edited by S. Kumar

Received: 23 December 2020 Revised: 8 September 2021 Accepted: 15 September 2021
Published online: 6 October 2021

[7, 11, 12]. Therefore, identifying molecular signals that regulate oncogenic dedifferentiation of hepatocytes, and non-parenchymal niches related to oncogenic and metastatic dedifferentiation, may represent a promising strategy to understand functional HCC development. However, the molecular mechanisms involved in the reprogramming of fully differentiated hepatocytes into a dedifferentiated state, have not been clearly demonstrated yet.

Ssu72 is a newly identified phosphatase with dual specificity and is associated with cell cycle control [13, 14] and liver homeostasis. Its depletion causes various liver diseases with high incidence [15]. However, the importance of Ssu72 phosphatase has been completely overlooked so far, although gene disruption studies have clearly demonstrated that there is no redundancy between Ssu72 and other phosphatases in liver diseases [15]. The present study provides important insights into steatohepatitis-associated HCC initiation and development, by hepatocyte dedifferentiation.

MATERIALS AND METHODS

Animals and treatments

$Ssu72^{flox/flox}$ ($Ssu72^{WT}$) mice were bred with C57BL/6J-cogenic albumin-Cre transgenic mice to generate liver-specific Ssu72 knockout mice ($Ssu72^{\Delta hep}$). $Ssu72^{WT}$ and $Ssu72^{\Delta hep}$ chimeric mice were established by cross-mating ROSA mTmG mice, generating $Ssu72^{WT}$; Rosa mTmG (hereafter $Ssu72^{ROSA;WT}$) and $Ssu72^{\Delta hep}$; ROSA mTmG (hereafter $Ssu72^{ROSA;\Delta hep}$). We also generated transgenic mice with a gene encoding HA-tagged Ssu72 in the ROSA26 locus. We then crossed these transgenic mice with $Ssu72^{\Delta hep}$ mice to generate $Ssu72^{\Delta hep}$; HA-Ssu72 mice. Two-week-old mice were injected with 25 mg/kg diethylnitrosamine (DEN). Tumor progression was then examined at 4, 7, and 10 months after injection with DEN. To induce NASH phenotypes, 5-week-old mice were fed a methionine-choline deficient (MCD) diet for 8 weeks or western plus fructose diet (high fat, high carbohydrates and high cholesterol) for 3 months. To induce hepatocyte dedifferentiation and oval cell proliferation, 5-week-old mice were fed a diet containing 0.1% 3,5-Diethoxycarbonyl-1,4-Dihydrocollidine (DDC).

Human cohort and treatment

A total of 604 resected paraffin-embedded tissues from patients with the following diagnoses: no diagnostic abnormalities (normal, $n = 10$), steatohepatitis ($n = 12$), mild fibrosis ($n = 70$), fibrotic or cirrhotic liver ($n = 105$), non-NASH-associated HCC ($n = 179$), or NASH-associated HCC ($n = 31$); were subjected to Ssu72 immunohistochemical staining using a Ventana Benchmark XT automated staining system. Ssu72 expression was scored by multiplying the staining intensity (0–3) and extent (%) in the cytoplasm of hepatocytes using Image J.

Histology, immunohistochemistry, and sirius red staining

Tissue samples were fixed in 10% formalin for 24 h at 4 °C, embedded in paraffin, sectioned (6 μm), and then stained with hematoxylin and eosin (H&E). For immunohistochemistry, deparaffinization of paraffin sections was conducted with xylene and ethanol. Heat-induced retrieval was performed by boiling sections in 10 mM citric acid buffer (pH 6.0) for 15 mins. Sections were then stained with antibodies at 4 °C followed by incubation with biotinylated secondary antibody (Vector) and visualization with 3,3′-diaminobenzidine. For Sirius Red staining, sections of formalin-fixed liver tissues were stained with 0.1% Sirius Red (Sigma-Aldrich) dissolved in saturated picric acid and then stained with H&E.

Oil Red O and immunofluorescence analyses

Liver cryosections were fixed with 4% paraformaldehyde and then stained with Oil Red O (Sigma-Aldrich) working solution for 1 h. These sections were washed twice with distilled water prior to visualization. For immunofluorescence analyses, tissues were fixed in 4% paraformaldehyde and incubated with indicated primary and secondary antibodies.

Isolation of hepatocytes and non-parenchymal cells and FACS analyses

Liver perfusion to isolate primary hepatocytes was conducted on 6-week-old male $Ssu72^{WT}$ mice using perfusion I buffer [142 mM NaCl, 6.7 mM KCl, 10 mM HEPES, and 16 mM EDTA (pH 7.4)] for 30 s and then perfusion II buffer [66.7 mM NaCl, 6.7 mM KCl, 10 mM HEPES, 4.8 mM $CaCl_2$, 0.0075% w/v 775U collagenase IV (Sigma-Aldrich), and 0.25% w/v FFA-free Albumin (GenDEPOT) (pH 7.6)] for 8 min. Hepatocytes were pelleted and purified using a Percoll gradient (40%). The non-parenchymal fraction was obtained as a supernatant from hepatocyte isolation. Freshly isolated non-parenchymal cells were stained with indicated antibodies. Stained cells were analyzed with a BD FACS Aria III analyzer (BD Biosciences) and Flowjo software.

Primary hepatocyte culture and treatment

Hepatocytes were cultured in William's E medium [2 mM L-glutamine, 25 mM HEPES, 100 nM dexamethasone, 100 nM insulin, 50 nM glucagon, 1% antibiotics (Welgene)] at 37 °C with 5% CO_2. Primary hepatocytes were treated with 500 μM palmitic acid and incubated for 6 h to mimic liver steatosis. 100 nM Okadaic acid (Abcam) was added to inhibit the phosphatase activity of primary hepatocytes for 1 h.

RNA isolation and quantitative real-time PCR

Total RNAs were isolated from liver tissues using an RNeasy Plus kit (Qiagen). cDNAs were then synthesized with an EasyScript cDNA synthesis kit (Abm) using random primers. Quantitative real-time PCR analyses were performed with SYBR Green on a Rotor Gene Q (Qiagen). Reactions were performed in triplicate. Relative gene expression was normalized to 5S rRNA gene and calculated using the comparative Ct ($2^{-\Delta\Delta Ct}$) method. Primer sequences used for qRT-PCR are shown in Supplementary Table 1.

RNA-seq and data analysis

RNA-Seq libraries were prepared from mRNA of isolated hepatocytes. Transcriptomic sequencing was performed on a NextSeq500 platform using standard protocol. A total of 50–160 million 76 base pair (bp) reads were generated per sample. An initial sequence-level quality assessment was performed using FastQC (Simon Andrews). RNA-Seq reads were then mapped to mouse mm10 reference genome using Tophat (v2.0.13), allowing a maximum of two mismatches per 75 bp sequencing. Differential gene expression analysis was performed using packages DESeq and edgeR. Data were obtained from two independent experiments and processed using DAVID Bioinformatics Resources 6.7 software for Gene ontology and KEGG pathway analysis.

Gene set enrichment analysis (GSEA)

Gene set enrichment analysis (GSEA) was carried out using the Broad Institute JAVA Desktop software (ver. 4.1.0) (www.broadinstitute.org/gsea) [16]. GSEA computationally calculates whether the members of the gene set show significant differences compared to controls using nonparametric Kolmogorov–Smirnov statistics. The annotated gene sets were acquired for the enrichment as either upregulation or downregulation from "hepatocytes" [17], "mammary stem cells" [18], and "changed gene in HNF4α depleted liver" [19] in microarray and RNA-Seq data. The normalized enrichment score (NES) was determined by investigating permutations 10,000 times. A $P < 0.10$ was considered to signify the statistical significance of an enriched gene set.

Chromatin immunoprecipitation (ChIP) analysis

For ChIP analysis, isolated hepatocytes were cross-linked with 1% formaldehyde for 20 min at room temperature. The reaction was then halted with 125 mM glycine. Hepatocytes were lysed with a lysis buffer (25 mM HEPES pH 8.0, 10 mM KCl, 0.1% NP-40, 1.5 mM $MgCl_2$, 1 mM DTT, and a protease inhibitor cocktail). Nuclei were isolated by re-suspending cells in lysis buffer for 30 min at 4 °C. Isolated nuclei were resuspended in a nuclei lysis buffer (50 mM HEPES pH 8.0, 140 mM NaCl, 1 mM EDTA, 1% Triton X-100, 0.1% sodium deoxycholate, 0.1% SDS, and a protease inhibitor cocktail) and sonicated with a Bioruptor Sonicator. Samples were then immunoprecipitated with appropriate antibodies in combination with Protein-G and -A Sepharose beads. Precipitates were extracted with elution buffer (10 mM Tris-HCl, pH 8.1, 1% SDS, 1 mM EDTA). Eluted samples were pooled and heated at 65 °C overnight to reverse formaldehyde cross-linking. qPCR reactions were performed with SYBR Green.

Immunoblotting and immunoprecipitation analyses

Tissues were prepared in RIPA buffer (150 mM NaCl, 1% Triton X-100, 0.1% SDS, 50 mM pH 7.5 Tris-HCl, 1% NP-40, 1 mM PMSF, 1 mM DTT and protease inhibitors). Equal amounts of protein lysates were separated by

SDS-PAGE and then transferred to nitrocellulose membranes. Membranes were blocked with 5% skim milk at room temperature for 1 h and then incubated with 5% skim milk overnight at 4 °C with antibodies. For immunoprecipitation analyses, liver extracts were lysed in buffer A [100 mM Tris-HCl (pH 7.5), 20 mM EDTA, 1% NP-40, 1 mM PMSF, 1 mM DTT, and protease inhibitor cocktail]. Supernatants (soluble cytoplasmic fractions) were obtained. Cell pellets were lysed in buffer B [100 mM Tris-HCl (pH 7.5), 20 mM EDTA, 300 mM NaCl, 1% NP-40, 1 mM PMSF, 1 mM DTT, and protease inhibitors] and briefly sonicated. Supernatants (soluble pellet fractions) were then obtained. Mixed extracts (soluble cytoplasmic and pellet supernatants) were diluted with a salt-free buffer to reduce salt concentration to 150 mM. Samples were then immunoprecipitated using appropriate antibodies in combination with Protein-A and -G agarose beads. Antibodies used are shown in Supplementary Table 2.

Cell transfection and GST pull-down analyses

HNF4α (NM_008261.3) DNA fragment was inserted in-frame into pcDNA3-GST plasmid DNA vector. To generate pcDNA3-GST-HNF4α mutants (phospho-mimic DBD, phospho-mimic hinge, and phospho-mimic LBD), site-directed mutagenesis was conducted using Muta-Direct™ site-directed mutagenesis kit (Lilif). HNF4α phospho-mimic mutant DBD has mutations in phosphorylation sites of the DNA binding domain (S87D, S95D, and S99D). HNF4α phospho-mimic mutant Hinge has mutations in phosphorylation sites of the hinge region (S142D, S143D, and S167D). HNF4α phospho-mimic LBD has mutations in phosphorylation sites of ligand binding domains (S190D, S262D, S265D, Y286D, S303D, S313D, and S318D) (Supplementary Fig. S13A, B). Phosphorylation sites of each domain were selected based on analysis using GPS 5.0 (www.gps.biocuckoo.org) kinase-specific phosphorylation site prediction and phosphositeplus® (www.phosphosite.org) [20–24]. Ssu72 (NM_014188.3) DNA fragment was inserted in-frame into pcDNA3-HA plasmid DNA vector. The plasmid DNA vector was delivered into primary hepatocytes by calcium phosphatase solution. The transfected primary hepatocytes were cultured for 24 h to express GST-HNF4α and HA-Ssu72. Primary hepatocytes were lysed in buffer C [20 mM Tris-HCl (pH 8.0), 100 mM NaCl, 1 mM EDTA (pH 8.0), 1 mM EGTA, 1% Triton X-100, 2.5 mM sodium pyrophosphate, 1 mM β-glycerophosphate, 1 mM Na_3VO_4, 1 mM PMSF and a protease inhibitor cocktail (GenDEPOT)], and briefly sonicated. Supernatants were then obtained and incubated with glutathione Sepharose 4B agarose beads (GE Healthcare) at 4 °C for 12 h.

Recombinant protein purification, in vitro kinase assay, and dephosphorylation analyses

PCR fragments of HNF4α (NM_000457.5) or Ssu72 (NM_014188.3) were inserted in-frame into pGEX-KG and pVFT1S plasmid DNA vector to express GST-fused HNF4α or His-fused Ssu72 protein in Rosetta *Escherichia coli* bacterial cells. To purify the GST-HNF4α, transformed Rosetta cells were incubated at 25 °C for 24 h with 0.01 mM IPTG. The cells were resuspended with STE buffer [10 mM Tris-HCl, 100 mM NaCl, 1 mM EDTA (pH 8.0), 0.1% Triton X-100 PMSF 1 mM, DTT 1 mM PMSF, and a protease inhibitor cocktail (pH 8.0)] and sonicated briefly. Supernatants were incubated with glutathione Sepharose 4B agarose beads at 4 °C for 4 h. His-Ssu72 was purified by incubating His-Ssu72 containing protein lysates with Ni-NTA agarose beads. For the in vitro kinase assay, bead-bound GST-HNF4α proteins were washed with kinase buffer [100 mM MOPS/NaOH (pH 7.2), 2 mM EDTA, 20 mM $MgCl_2$, 1 mM DTT and 1 mM PMSF] and incubated with 1 μg of recombinant AMPK proteins (Sigma-Aldrich) containing 1 mM ATP at 37 °C for 1 h. For the HNF4α dephosphorylation assay, phosphorylated GST-HNF4α proteins were washed twice with phosphatase buffer [100 mM MOPS/NaOH (pH 7.2), 10 mM $MgCl_2$, 0.1 mM $ZnCl_2$, 2 mM EGTA] and incubated with purified His-Ssu72 WT or His-Ssu72 C12S (phospho-dead Ssu72 mutant) proteins at 30 °C for 6 h.

Statistical analysis

Results were analyzed using Student's *t* test or analysis of variance (ANOVA) as appropriate using GraphPad Prism software. A Bonferroni post hoc test was used to test for significant differences as determined by ANOVA. Data are presented as mean ± standard error of the mean (SEM). Significance was accepted at $p \le 0.05$. Levels of significance are indicated by asterisks ($*p \le 0.05$; $**p < 0.01$; $***p < 0.001$; $****p < 0.0001$).

RESULTS

Relationship between loss of Ssu72 phosphatase and NASH-associated HCC development

Our previous study revealed that hepatic Ssu72 depletion can lead to a high incidence of NAFLD and NASH development in mice, even without metabolic syndrome-inducing conditions, but was not associated with spontaneous HCC development [15]. Thus, we wanted to know why there were no HCC lesions in Ssu72-depleted ($Ssu72^{\Delta hep}$) mice despite various NAFLD and NASH lesions that persisted for a long period (Fig. 1A, B and Supplementary Fig. S1A). Next, dominant histopathological features of liver commonly described in NASH, including steatosis, lobular inflammation, hepatocyte ballooning, and even mild fibrosis, were scored according to NASH activity score (NAS) system (Fig. 1B and Supplementary Fig. S1B, C). In $Ssu72^{WT}$ livers, total NAS score (sum of steatosis, lobular inflammation and hepatocyte ballooning) was below 2. However, it was significantly increased after Ssu72 depletion. We further observed a striking increase of total NAS score exceeding 7 in $Ssu72^{\Delta hep}$ mice (Supplementary Fig. S1C). Fibrosis scores were also remarkably increased after Ssu72 depletion (Supplementary Fig. S1B, C). However, the development of dysplastic nodules or HCC following advanced NASH phenotype were not observed in $Ssu72^{\Delta hep}$ mice (Supplementary Fig. S1A). To further investigate the correlation between Ssu72 expression and NASH phenotype, MCD diet was administrated to $Ssu72^{WT}$ and $Ssu72^{\Delta hep}$ mice to boost their NASH symptoms. Severity scores of NASH phenotypes including ballooning, lipid droplet accumulation, fibrosis, and immune cell infiltration were drastically increased by MCD diet in Ssu72-depleted mice (Fig.1C and Supplementary Fig. S1D, E). In addition, metabolic syndrome-induced $Ssu72^{\Delta hep}$ mice fed with western + fructose diet rapidly developed NASH with severe fibrosis (Supplementary Fig. S1F). To further evaluate the crosstalk between human Ssu72 and NASH symptoms, Ssu72 expression levels were compared between normal human liver samples and patient specimens. Most normal liver samples exhibited high levels of Ssu72 expression. Ssu72 expression was particularly high in periportal hepatocytes, more so than in pericentral hepatocytes (Fig. 1D). However, Ssu72 expression was significantly downregulated in steatohepatitis, viral hepatitis, alcoholic hepatitis, fibrosis, cirrhotic liver, and even in HCC specimens (Fig. 1D–F and Supplementary Fig. S2A and Supplementary Table 3). Significantly, we found that Ssu72 expression was markedly decreased in NASH-associated HCC specimens compared to non-NASH-associated HCC (Fig. 1G). In cholangiocytes, there were no significant differences in Ssu72 expression in normal, inflammatory, and tumor regions (Supplementary Fig. S2B). These results indicate that downregulation of Ssu72 is closely associated with not only the development of NASH but also with alcoholic steatohepatitis (ASH) and viral hepatitis.

Loss of Ssu72 leads to marked susceptibility to HCC development in various chemical and metabolic syndrome-induced models

We questioned whether hepatic Ssu72 might be associated with HCC initiation and development. Accordingly, we administered procarcinogen DEN to 2-week-old $Ssu72^{WT}$ and $Ssu72^{\Delta hep}$ mice and observed a striking difference in HCC development between the two models (Fig. 2A). Both macroscopic and microscopic examination revealed dramatic increases in weight, number, and size of tumor foci in the livers of $Ssu72^{\Delta hep}$ mice compared to $Ssu72^{WT}$ littermates (Fig. 2A–C). Based on histopathologic tumor features from 10-month-old DEN-challenged $Ssu72^{WT}$ and $Ssu72^{\Delta hep}$ livers, DEN-challenged $Ssu72^{\Delta hep}$ livers clearly exhibited more advanced high-grade HCC and remarkable anaplasia of HCC with intrahepatic cholangiocarcinoma (HCC–ICC) (Fig. 2D). Interestingly, $Ssu72^{\Delta hep}$ liver exhibited dysplastic nodules, adenoma, and HCC within 4 months of DEN administration while $Ssu72^{WT}$

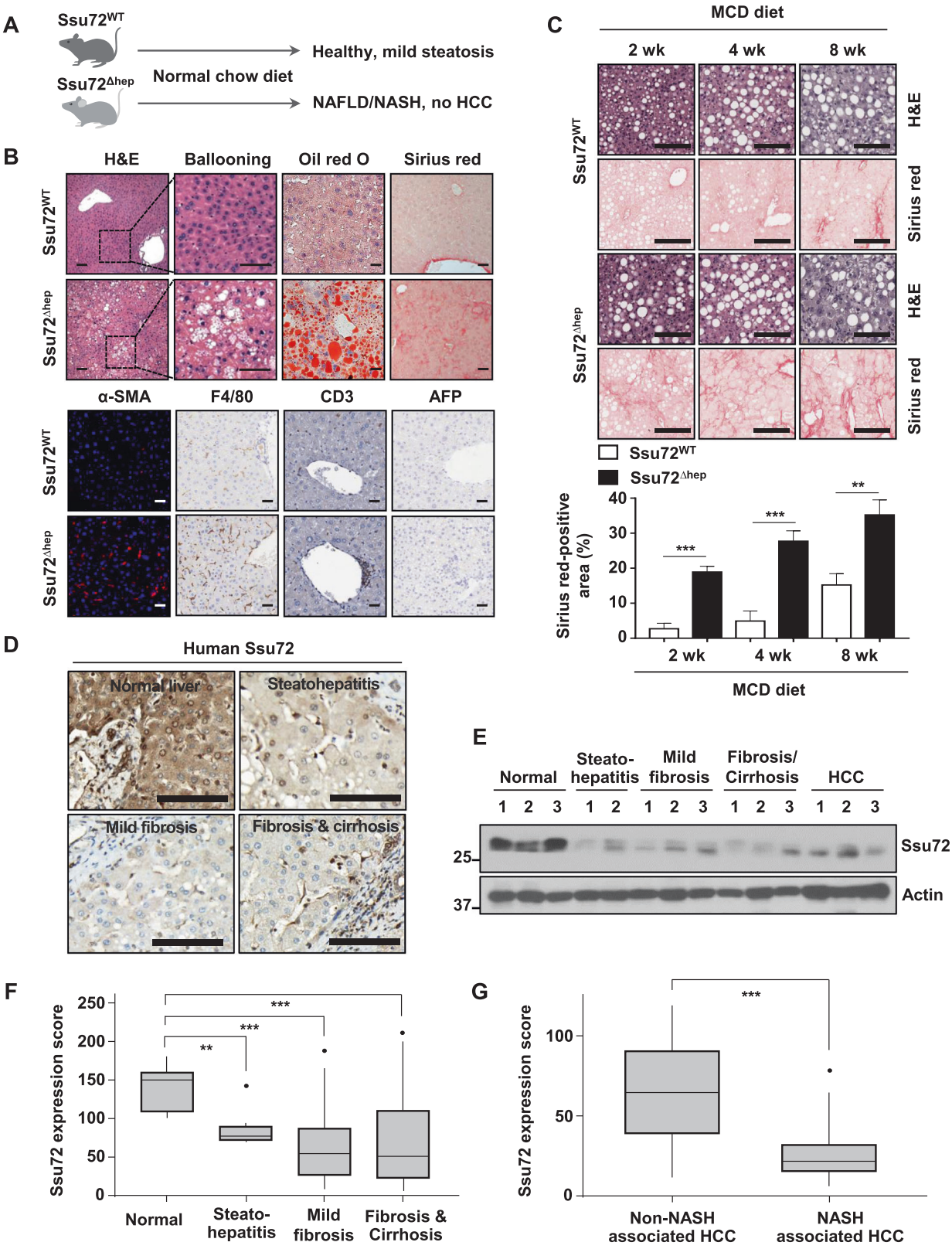

liver did not show tumor formation until 4 months after DEN, indicating that Ssu72 depletion was closely linked to susceptibility to HCC development (Fig. 2A–D). Furthermore, $Ssu72^{WT}$ and $Ssu72^{\Delta hep}$ mice were administered streptozotocin (STZ) known to be toxic to pancreatic insulin-producing β cells at postnatal day 2, followed by HFD feeding (STAM model, Fig. 2E) [25]. As expected, after combined administration of STZ and HFD feeding, weight (data not shown), number, and size of tumor foci were sharply increased in livers of $Ssu72^{\Delta hep}$ compared to $Ssu72^{WT}$ mice (Fig. 2F), indicating that Ssu72 depletion resulted in marked

Fig. 1 Loss of Ssu72 leads to high incidence of NAFLD/NASH. A Schematic representation of liver phenotypes of $Ssu72^{WT}$ and $Ssu72^{\Delta hep}$ mice fed with a normal chow diet (scale bars = 100 μm). **B** Representative pictures of H&E and IHC analyses for Oil red O, Sirius red, α-SMA, F4/80, CD3, and AFP staining of $Ssu72^{WT}$ and $Ssu72^{\Delta hep}$ livers at 52 weeks of age (scale bars = 100 μm). **C** Six-week-old $Ssu72^{WT}$ and $Ssu72^{\Delta hep}$ mice were fed an MCD diet for 2, 4, and 8 weeks. Liver sections from MCD-challenged $Ssu72^{WT}$ and $Ssu72^{\Delta hep}$ mice were subjected to H&E and Sirius red staining (upper) (scale bars = 100 μm). Quantification of Sirius red signals using Image J (bottom). Data are presented as mean ± SEM. Statistical analyses were conducted by t-test (**$p < 0.01$ and ***$p < 0.001$). **D** Ssu72 IHC of representative sections of human normal, steatohepatitis, mild fibrosis, and fibrotic/cirrhotic liver tissues (scale bars = 100 μm). **E** Liver extracts of normal, steatohepatitis, mild fibrosis, and fibrotic/cirrhotic liver tissues were immunoblotted with anti-Ssu72 and anti-actin antibodies. **F** Intensity and extent of Ssu72 expression were determined microscopically using IHC scorings defined as the sum of staining intensity (score of 0–3) multiplied by the percentage of cells (0–100) stained at a given intensity [no diagnostic abnormalities ($n = 10$), steatohepatitis ($n = 12$), mild fibrosis ($n = 70$), and fibrosis/cirrhosis liver specimens ($n = 105$)]. Data are presented as mean ± SEM. Statistical analyses were conducted by two-way ANOVA (**$p < 0.01$ and ***$p < 0.001$). **G** Ssu72 expression was scored by multiplying the staining intensity (0–3) and extent (%) using Image J [non-NASH-associated HCC ($n = 179$), NASH-associated HCC ($n = 31$)]. Data are presented as mean ± SEM. Statistical analyses were conducted by t-test (***$p < 0.001$). See also Supplementary Figs. S1, 2.

susceptibility to HCC development in the context of metabolic syndrome.

Histological analyses showed that both tumor and non-tumor regions of DEN-challenged $Ssu72^{\Delta hep}$ livers, had NASH lesions such as ballooning, lipid droplet accumulation, and macrophage infiltration at 4 months following DEN challenge (Fig. 2G and Supplementary Fig. S3A, B). These lesions were increasingly apparent at 10 months post-DEN, whereas DEN-challenged $Ssu72^{WT}$ livers showed simple steatosis and mild macrophage infiltration in both the tumor and non-tumor areas (Fig. 2G and Supplementary Fig. S3B). Additionally, P62 expression levels (known to be associated with increased ER stress and tumorigenesis) and aberrant fibrosis were significantly increased in DEN-challenged $Ssu72^{\Delta hep}$ liver compared to DEN-challenged $Ssu72^{WT}$ (Fig. 2G, H and Supplementary Fig. S3A, B). Indeed, DEN-challenged $Ssu72^{\Delta hep}$ livers exhibited induction of both inflammation and fibrosis-related genes compared to $Ssu72^{WT}$ livers (Supplementary Fig. S3C). Furthermore, DEN-challenged $Ssu72^{\Delta hep}$ mice showed increased levels of triglyceride, cholesterol, AST, and ALT in both serum and liver (Supplementary Fig. S3D). We confirmed that $Ssu72^{\Delta hep}$ livers showed advanced NASH phenotypes in the context of metabolic syndrome (STAM model) (Fig. 2I and Supplementary Fig. S3E). Taken together, these results suggest that Ssu72 depletion can lead to enhanced susceptibility to transition from NASH to NASH-associated HCC and malignant HCC progression.

Marked increment of the hepatic progenitor pool in Ssu72-deleted liver in response to liver damage

To understand what induced malignant HCC development in $Ssu72^{\Delta hep}$ livers, we compared functional alterations to $Ssu72^{WT}$ and $Ssu72^{\Delta hep}$ hepatocytes in response to DEN challenge. DEN is known to be preferentially metabolized in Cyp2E1-expressing hepatocytes around the central vein [26, 27], thereby inducing injury and proliferation [9]. Although the presence or absence of Ssu72 had little effect on proliferation of hepatocytes in unchallenged livers, DEN administration resulted in a remarkable increase in the population of proliferating oval-shaped cells with the morphology of biliary epithelial cells in pericentral zones of Ssu72-depleted livers (Fig. 3A). Additionally, the majority of these cells were positive for the proliferation marker PCNA (Fig. 3A).

To identify relevant features of proliferating oval-shaped cells, we performed immunohistochemical analyses for progenitor markers. IHC results revealed that Sox9 and Epcam were expressed only in bile ductal and marginal oval-shaped cells throughout $Ssu72^{WT}$ livers after DEN challenge, whereas their populations were rapidly increased in DEN-challenged $Ssu72^{\Delta hep}$ livers, showing strongly expressed progenitor markers in both pericentral and periportal zones (Fig. 3B and Supplementary Fig. S4A). Upon damage, FSCs (also known as oval cells) showed characteristics of expanded bile duct cells known to express Notch1 and Yap1 signaling proteins [28]. Increased numbers of oval-shaped cells in DEN-challenged $Ssu72^{\Delta hep}$ livers also expressed Jag1 and Yap1 (Fig. 3B and Supplementary Fig. S5A). However, the expression of hepatocyte marker HNF4α was undetectable in these oval-shaped cells (Supplementary Fig. S5A). In addition, there were no differences in expression of cell death markers RIP1, p-RIP3, and cleaved-caspase3 in DEN-challenged $Ssu72^{WT}$ and $Ssu72^{\Delta hep}$ livers, whereas the expression of oxidative stress marker 4-HNE was remarkedly increased in DEN-challenged $Ssu72^{\Delta hep}$ liver compared to $Ssu72^{WT}$ (Supplementary Fig. S5B, C). These results imply that Ssu72 depletion does promote oxidative damage, which may be stimulated by the proliferation of oval-shaped cells.

We next performed FACS analyses for progenitor markers. $Ssu72^{WT}$ and $Ssu72^{\Delta hep}$ mice were treated with DEN to induce oval-shaped cells. Ssu72-deficient cells showed markedly higher proportions of cells positive for biliary and progenitor markers compared to $Ssu72^{WT}$ (Supplementary Fig. S6A). Given the immunohistochemical characteristics of oval-shaped cells, we hypothesized that they might be involved in the population of non-parenchymal cells. Thus, we isolated non-parenchymal cells from DEN-challenged $Ssu72^{WT}$ and $Ssu72^{\Delta hep}$ mice using Percoll (Fig. 3C). Before DEN administration, no significant change was seen for Epcam-positive but CD11b-negative progenitor cells ($Epcam^{+}CD11b^{-}$) between $Ssu72^{WT}$ and $Ssu72^{\Delta hep}$ livers (Fig. 3C). Strikingly, in response to DEN damage, $Epcam^{+}CD11b^{-}$ progenitor cells in $Ssu72^{\Delta hep}$ livers were dramatically increased compared to those in $Ssu72^{WT}$ livers (Fig. 3C). In accordance with this observation, we also found significant induction of $Sox9^{+}CD11b^{-}$ and $CD13^{+}CD133^{+}$ cells in the population of non-parenchymal cells in DEN-challenged $Ssu72^{\Delta hep}$ livers (Supplementary Fig. S6B, C). In additional, we confirmed the above results with a STAM model in the context of metabolic syndrome. We found strong induction of $Sox9^{+}$ and $Epcam^{+}$ cells in STAM-challenged $Ssu72^{\Delta hep}$ livers (Fig. 3D and Supplementary Fig. S6D). Taken together, these results indicate that Ssu72 depletion can result in a marked increase in the number of proliferating oval-shaped cells (hepatic progenitor cells) in response to chemical and metabolically induced-liver damage.

Loss of hepatic Ssu72 induces hepatocyte-to-hepatic progenitor cell conversion

Based on previous reports our results could have two explanations. First, Ssu72 depletion can lead to dedifferentiation of hepatocytes into progenitor cells. Second, Ssu72 depletion can induce expansion of FSCs that reside in the periportal region. To clarify these two possibilities, we established $Ssu72^{WT}$ and $Ssu72^{\Delta hep}$ chimeric mice by cross-mating with ROSA mTmG mice, generating $Ssu72^{WT}$; ROSA mTmG (hereafter $Ssu72^{ROSA;WT}$) and $Ssu72^{\Delta hep}$; ROSA mTmG (hereafter $Ssu72^{ROSA;\Delta hep}$) mice, respectively (Fig. 4A). When albumin-Cre or thyroid hormone-binding globulin (TBG)-Cre was not present, mTmG mice constitutively expressed tdTomato in all liver cells. In contrast, when mTmG mice

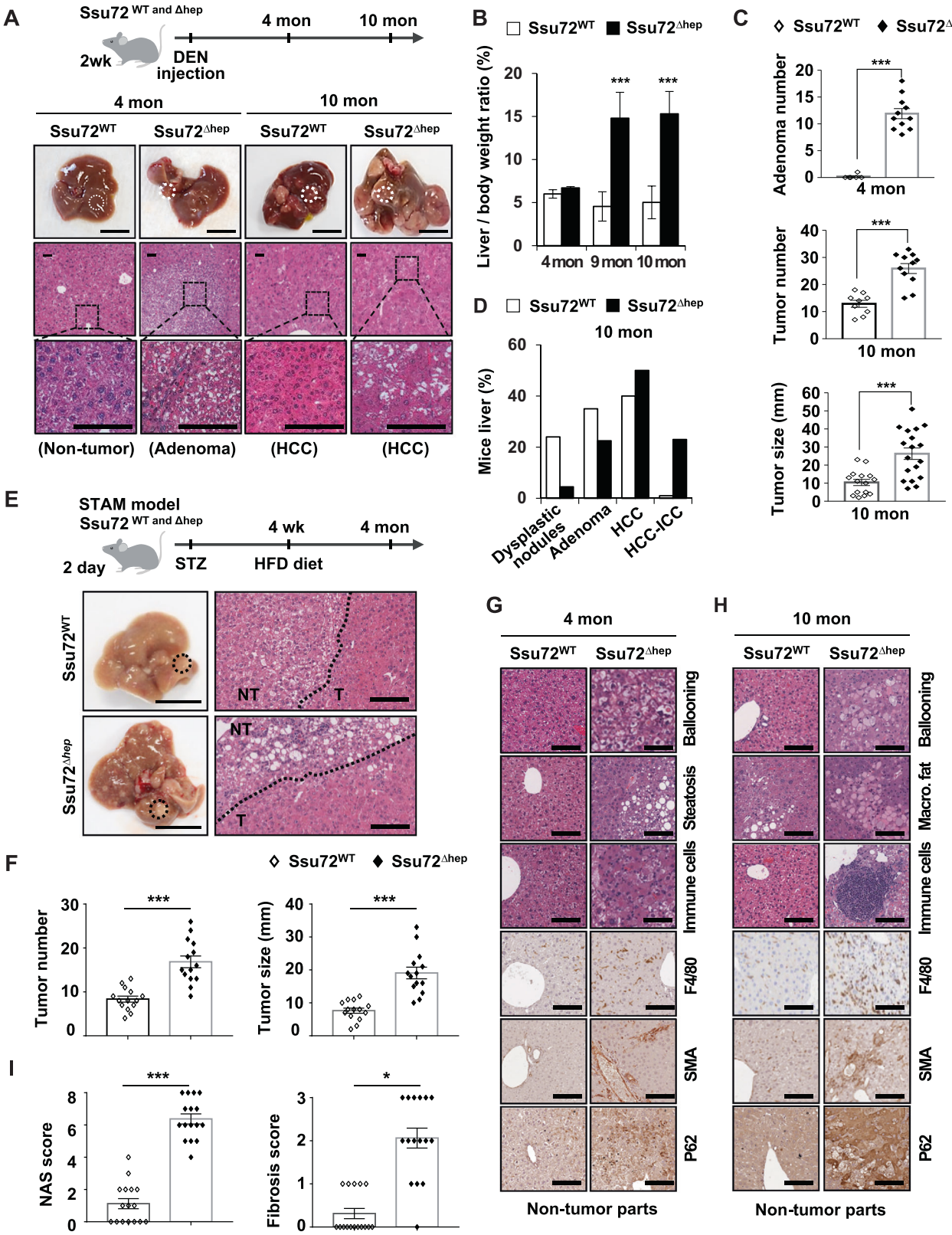

were exposed to albumin-Cre or TBG-Cre, the tdTomato expression cassette was excised and rearranged for GFP expression and subsequent green color expression (Supplementary Fig. S7A). Both tdTomato and GFP are membrane-targeted, allowing for delineation of single cells and cell processes by confocal microscopy. We decided to take advantage of this system to specifically track the fate of Ssu72-depleted hepatocytes and FSCs after liver injury. Following 5 days post-DEN challenge, the morphologies of pericentral areas in $Ssu72^{ROSA;WT}$ were considerably restored (Fig. 4B). Sox9-positive cells in pericentral areas were barely

Fig. 2 Loss of Ssu72 leads to marked susceptibility to HCC development in various chemical and metabolic syndrome-induced models. **A** Two-week-old $Ssu72^{WT}$ and $Ssu72^{\Delta hep}$ mice were intraperitoneally injected with DEN (25 mg/kg) and examined at 4 and 10 months after injection [4 months: ($Ssu72^{WT}$: $n = 10$, $Ssu72^{\Delta hep}$: $n = 11$); 10 months: ($Ssu72^{WT}$: $n = 12$, $Ssu72^{\Delta hep}$: $n = 14$)]. Gross morphology (scale bar = 1 cm) and H&E staining of 4 and 10-month-old DEN-challenged $Ssu72^{WT}$ and $Ssu72^{\Delta hep}$ livers (scale bar = 100 μm). **B** Histopathologic classification of various tumor types from 10-month-old DEN-challenged $Ssu72^{WT}$ and $Ssu72^{\Delta hep}$ livers. Data are presented as mean ± SEM. Statistical analyses were conducted by t-test (***$p < 0.001$). **C**, **D** Macroscopic and microscopic tumor developments were determined 10 months after DEN administration. Tumor includes dysplastic nodules, adenoma, HCC, and ICC. Data are presented as mean ± SEM. Statistical analyses were conducted by t-test (***$p < 0.001$) Numbers of mice: ($Ssu72^{WT}$: $n = 12$, $Ssu72^{\Delta hep}$: $n = 14$). Number of tumor sections: ($Ssu72^{WT}$: $n = 24$, $Ssu72^{\Delta hep}$: $n = 34$). **E**, **F** Two-day-old $Ssu72^{WT}$ and $Ssu72^{\Delta hep}$ mice were intraperitoneally injected with streptozotocin (STZ, 200 μg) and mice were fed a high-fat diet (HFD) for 4 months [(STAM model, $n = 10$ ($Ssu72^{WT}$) and $n = 12$ ($Ssu72^{\Delta hep}$)]. **E** Gross morphology (scale bar = 1 cm) and H&E staining of representative sections from livers of STAM-challenged $Ssu72^{WT}$ and $Ssu72^{\Delta hep}$ mice (scale bar = 100 μm). **F** Macroscopic and microscopic tumor developments (tumor numbers and size) were determined at 4 months after STAM administration. Data are presented as mean ± SEM. Statistical analyses were conducted by t-test (*$p \leq 0.05$ and ***$p < 0.001$) **G**, **H** Representative H&E and IHC staining of non-tumor areas from DEN-challenged $Ssu72^{WT}$ and $Ssu72^{\Delta hep}$ livers (scale bar = 100 μm). **I** Histopathological NAS and fibrosis scores of STAM-challenged $Ssu72^{WT}$ and $Ssu72^{\Delta hep}$ mice. Scatter dots are individual liver sections [$Ssu72^{WT}$ and $Ssu72^{\Delta hep}$, respectively ($n = 8$)]. See also Supplementary Fig. S3.

detected in $Ssu72^{ROSA;WT}$ liver, whereas Sox9-positive progenitor-like cells were significantly increased in the pericentral areas of DEN-damaged $Ssu72^{ROSA;\Delta hep}$ liver (Fig. 4B). Similar results were observed in AAV-TBG-Cre infected $Ssu72^{ROSA;f/f}$ livers (Fig. 4C). These cells were highlighted in green by albumin-Cre or TBG-Cre at baseline, implying that GFP^+ progenitor-like cells observed after DEN challenge could be derived from mature hepatocytes (Fig. 4B, C). To further evaluate the fate of GFP and Sox9-positive progenitor-like cells after albumin-Cre or TBG-Cre administration, we performed immunostaining of Ck19 as a marker for biliary and progenitor cells at day 5 post-DEN challenge (Supplementary Fig. S7B, C). As expected, GFP^+ and $Ck19^+$ (double positive) cells were markedly increased in Ssu72-depleted mature hepatocytes (Supplementary Fig. S7B, C). Taken together, these results imply that Ssu72 expression level is closely associated with cell fate of hepatocytes following liver damage, and that down-regulation of Ssu72 could potentiate the induction of hepatocyte dedifferentiation.

To explore the impact of Ssu72 deficiency on hepatocyte dedifferentiation, we adopted an activation system for progenitor or oval cells by feeding mice a 3,5-diethoxycarbonyl-1,4-dihydrocollidine (DDC) diet known to induce hepatocyte dedifferentiation [7]. DDC diet induced an increase in progenitor and/or oval cells and a ductular reaction, which were significantly increased in $Ssu72^{ROSA;\Delta hep}$ liver compared to $Ssu72^{ROSA;WT}$ (Fig. 4D and Supplementary Fig. S7D). Notably, the number of $Ki67^+$ oval cells was drastically increased in DDC-challenged $Ssu72^{ROSA;\Delta hep}$ livers (Fig. 4D). This effect appeared to be linked to increased liver weights of DDC-challenged $Ssu72^{ROSA;\Delta hep}$ mice (Supplementary Fig. S7E). To characterize the cellular identity of increased oval and ductal cells induced by DDC administration, we performed immunostaining for Sox9 and ductal marker A6 (Fig. 4E, F). Importantly, the majority of new oval- and ductal-like cells in DDC-challenged $Ssu72^{ROSA;WT}$ and AAV-TBG-Cre infected $Ssu72^{ROSA;+/+}$ livers were marked with tdTomato, whereas GFP^+ oval and ductal-shaped cells that originated from hepatocytes in DDC-challenged $Ssu72^{ROSA;\Delta hep}$ and AAV-TBG-Cre infected $Ssu72^{ROSA;f/f}$ livers were strongly positive for Sox9 and A6 (Fig. 4E, F), implying that these Ssu72-depleted oval- and ductal-like cells were derived from dedifferentiated hepatocytes. To further examine the relationship between chronic hepatic damage-induced tumorigenesis and lineage-related alterations in the conversion from hepatocytes into progenitor cells, both $Ssu72^{ROSA;WT}$ and $Ssu72^{ROSA;\Delta hep}$ mice were administrated with long-term DDC diet (Supplementary Fig. S8 and Supplementary Fig. S16B). The administration of DDC for 10 weeks moderately induced the activation of oval cells in $Ssu72^{ROSA;WT}$ livers, whereas DDC-challenged $Ssu72^{ROSA;\Delta hep}$ livers showed development of small dysplastic nodules. These nodules developed into HCC at 20–45 weeks after DDC (Supplementary Fig. S8). We also found that tumor areas in NASH-associated HCC caused by Ssu72 depletion significantly induced HCC and progenitor markers, indicating that hepatic progenitor potential induced by Ssu72 loss may contribute to distinct pathogenic fates resulting in either NASH or NASH-associated HCC (Supplementary Fig. S9). Together, these data support the conclusion that chronic hepatic damage caused by DDC diet can induce significant hepatocyte transition to progenitor cells in $Ssu72^{\Delta hep}$ livers.

Hepatic Ssu72 regulates HNF4α-mediated transcription signaling in response to liver damage

Based on our RNA-seq and GSEA (Supplementary Fig. S10A–C and Supplementary Table 4), we found that about 45% of down-regulated gene subsets in $Ssu72^{\Delta hep}$ hepatocytes belonged to gene targets of HNF4α which is a critical transcription factor for maintenance of hepatocyte function (Fig. 5A). GSEA consistently showed that gene signatures in HNF4α depleted liver were closely correlated to those in DEN-challenged $Ssu72^{\Delta hep}$ hepatocytes (Fig. 5B). These results imply that hepatic Ssu72 contributes to the accurate modulation of HNF4α target genes under conditions of liver damage. Furthermore, IHC analyses also revealed that SALL4, as an oncofetal and progenitor property gene [29, 30] was significantly increased in the pericentral zone of $Ssu72^{\Delta hep}$ liver (Supplementary Fig. S11A). In addition, about 39% of gene subsets upregulated in $Ssu72^{\Delta hep}$ hepatocytes belong to gene targets of E2F, indicating that Ssu72 loss could lead to recovery of the ability to proliferate through damage-mediated dedifferentiation (Our unpublished observation).

qRT-PCR analysis demonstrated that loss of Ssu72 had a tendency to downregulate HNF4α target genes (Fig. 5C). To examine the clinical relevance of the Ssu72 and HNF4α interaction, we evaluated expression levels of these proteins in paired tissues obtained from 28 patients with NASH-associated HCC. HCC patients with weak expression of Ssu72 showed parallel low expression of HNF4α in the same tissues, and vice versa (Fig. 5D). The correlation between Ssu72 and HNF4α was further analyzed in patients with NASH and/or cirrhosis. Again, close positive correlations between Ssu72 and HNF4α expression levels were found for patients with steatohepatitis, mild fibrosis, and fibrosis/cirrhosis (Fig. 5E).

We next examined the correlation between Ssu72 and HNF4α expression in primary hepatocytes. Isolated primary hepatocytes were infected with adenovirus expressing GFP or Cre recombinase. Hepatocytes were cultured with palmitic acid to induce lipotoxicity. Consistently, we found that depletion of Ssu72 diminished HNF4α mRNA and protein level in primary hepatocytes (Supplementary Fig. S12A, B). As in human patients the levels of Ssu72 and HNF4α were reduced in palmitic acid-treated primary hepatocytes. The phosphorylation of HNF4α was increased in Ssu72-depleted primary hepatocytes, and in particular palmitic acid-treated primary hepatocytes exhibited greater HNF4α phosphorylation than untreated hepatocytes (Supplementary Fig. S12B). Of note, the Ser 313 phosphorylation site of HNF4α is

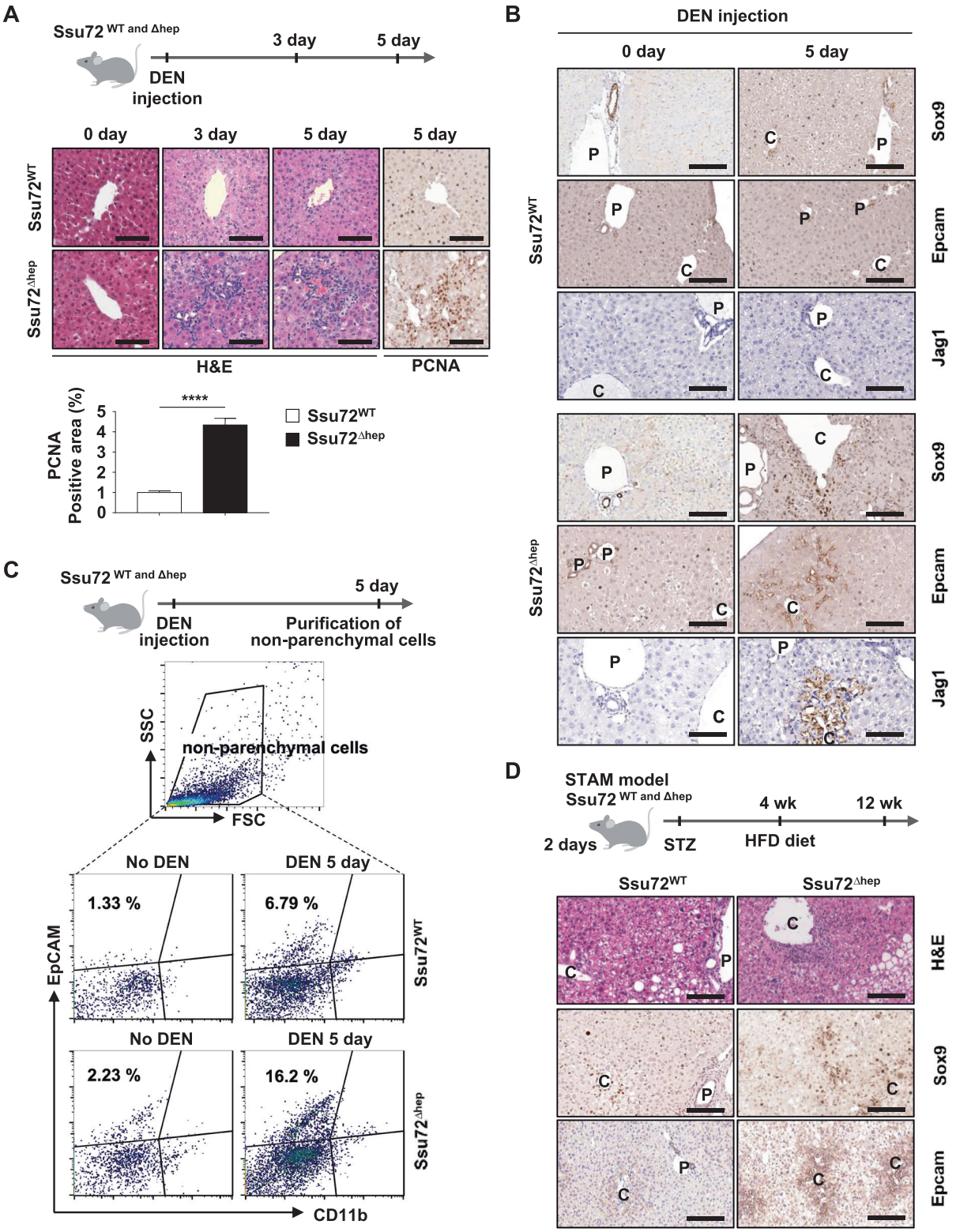

Fig. 3 Marked increase of hepatocyte proliferation potential in Ssu72-deleted livers in response to liver damage. A Six-week-old $Ssu72^{WT}$ and $Ssu72^{\Delta hep}$ mice were intraperitoneally injected with DEN (150 mg/kg) and examined after 3 and 5 days ($n > 15$ mice per group). H&E staining, IHC staining and PCNA positive area quantified from DEN-challenged $Ssu72^{WT}$ and $Ssu72^{\Delta hep}$ livers (scale bar = 100 μm). Data are presented as mean ± SEM. Statistical analyses were conducted by t-test (****$p < 0.0001$). **B** Sox9, Epcam, and Jag1 IHCs of DEN-challenged $Ssu72^{WT}$ and $Ssu72^{\Delta hep}$ livers (C: pericentral vein, P: periportal vein) (scale bar = 100 μm). **C** Schematic representation of non-parenchymal cells isolated from DEN-challenged $Ssu72^{WT}$ and $Ssu72^{\Delta hep}$ mice. FACS plots of Epcam expression in non-parenchymal cells from DEN-challenged $Ssu72^{WT}$ and $Ssu72^{\Delta hep}$ livers. **D** Two-day-old $Ssu72^{WT}$ and $Ssu72^{\Delta hep}$ mice were intraperitoneally injected with STZ and mice were fed a high-fat diet (HFD) for 2 months [(STAM model, $n = 7$ ($Ssu72^{WT}$) and $n = 10$ ($Ssu72^{\Delta hep}$)]. H&E staining, and Sox9 and Epcam IHC of STAM-challenged $Ssu72^{WT}$ and $Ssu72^{\Delta hep}$ livers (scale bar = 100 μm). See also Supplementary Figs. S4–6.

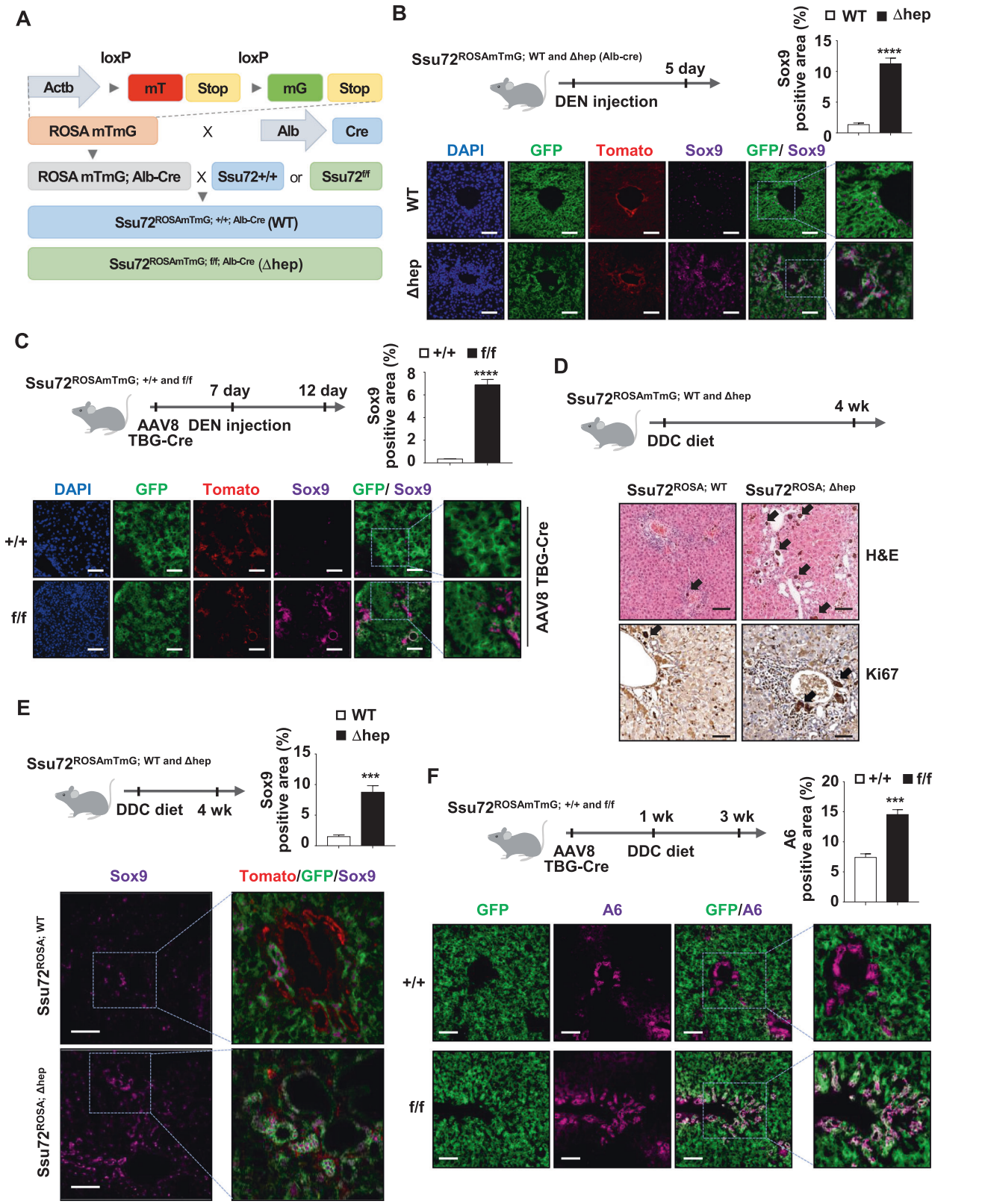

known to inhibit its transcriptional activity [21]. Collectively, these data indicate that Ssu72 is highly downregulated in NASH and HCC patients, potentially through its association with HNF4α expression and this has profound effects on the regulation of HNF4α by phosphorylation.

Ssu72 negatively regulates hepatocyte oncogenic proliferation/dedifferentiation by activating HNF4α mediated transcription

HNF4α is a master transcriptional regulator of functional liver maintenance. HNF4α is markedly downregulated in NASH, ASH,

Fig. 4 Loss of hepatic Ssu72 results in induction of hepatocyte-to-progenitor cell conversion. A ROSA mTmG mice were crossed with albumin-Cre (Alb-Cre) mice. Resulting mice were intercrossed with $Ssu72^{+/+}$ or $Ssu72^{f/f}$ mice to generate $Ssu72^{+/+}$; ROSA mTmG; Alb-Cre ($Ssu72^{ROSAmTmG;WT}$, WT) and $Ssu72^{f/f}$;ROSA mTmG;Alb-Cre ($Ssu72^{ROSAmTmG;\Delta hep}$, Δhep) mice. **B** Six-week-old $Ssu72^{ROSAmTmG;WT}$ and $Ssu72^{ROSAmTmG;\Delta hep}$ mice were intraperitoneally injected with 150 mg/kg DEN. After 5 days, liver sections were immunostained for Sox9 (scale bar = 100 μm). Data are presented as mean ± SEM. Statistical analyses were conducted by t-test (****$p < 0.0001$). **C** Five-week-old $Ssu72^{ROSAmTmG;+/+}$ and $Ssu72^{ROSAmTmG;f/f}$ mice were intravenously injected with AAV8-TBG-Cre (1×10^{11} gene copies per mouse). After 7 days, $Ssu72^{ROSAmTmG;+/+}$ and $Ssu72^{ROSAmTmG;f/f}$ mice were intraperitoneally injected with DEN (150 mg/kg) and examined after 5 days. Liver sections were immunostained for Sox9 (scale bar = 100 μm). Data are presented as mean ± SEM. Statistical analyses were conducted by t-test (****$p < 0.0001$). **D** H&E and Ki67 IHC analyses of DDC-challenged $Ssu72^{ROSAmTmG;WT}$ and $Ssu72^{ROSAmTmG;\Delta hep}$ livers (scale bar = 100 μm). The arrows denote bile acid stasis. **E** Liver sections from DDC-challenged $Ssu72^{ROSAmTmG;WT}$ and $Ssu72^{ROSAmTmG;\Delta hep}$ mice were immunostained for Sox9 (scale bar = 100 μm). Data are presented as mean ± SEM. Statistical analyses were conducted by t-test (***$p < 0.001$). **F** AAV8-TBG-Cre-challenged $Ssu72^{ROSAmTmG;+/+}$ and $Ssu72^{ROSAmTmG;f/f}$ mice were fed a DDC diet for two weeks. Liver sections from mice were immunostained for for A6 (scale bar = 100 μm). Data are presented as mean ± SEM. Statistical analyses were conducted by t-test (***$p < 0.001$). See also Supplementary Figs. S7–9.

cirrhotic liver, and hepatoma development [31]. Notably, the transcriptional activity of HNF4α is predominantly regulated by phosphorylational modification [32]. To verify relationships between HNF4α and Ssu72, we examined their phosphorylation levels after DEN challenge (Fig. 6A). As expected, DEN markedly induced HNF4α phosphorylation in $Ssu72^{WT}$ livers as evidenced by mobility shift on a phospho-tag gel (Fig. 6A). Importantly, HNF4α hyper-phosphorylation was partially restored within 5 days after DEN administration in $Ssu72^{WT}$ livers (Fig. 6A). Surprisingly, hyper-phosphorylated forms of HNF4α in DEN-challenged $Ssu72^{\Delta hep}$ livers were consistently maintained for 5 days after DEN administration without activation of kinases such as AMPKα, which is known to phosphorylate Ser 304 of HNF4α during liver damage (Fig. 6A and Supplementary Fig. S13A). IHC analyses also revealed that HNF4α was hyper-phosphorylated in DEN-challenged $Ssu72^{\Delta hep}$ livers (Fig. 6B). This result raises the possibility that Ssu72 may directly counteract or antagonize the hyper-phosphorylation of HNF4α, thereby contributing to the restoration of its phosphorylation caused by hepatic damage. We therefore examined whether Ssu72 could physically bind to HNF4α. Immunoprecipitation assay revealed that Ssu72 interacted with HNF4α during DEN-injury, implying that Ssu72 might selectively form a complex with hyper-phosphorylated HNF4α (Fig. 6C). To define the interaction between Ssu72 and HNF4α more clearly, purified GST-fused HNF4α (GST-HNF4α) bound to agarose beads was incubated with His-Ssu72 (WT) or His-Ssu72 (C12S) mutant. Purified His-fused Ssu72 WT (His-Ssu72 WT) physically bound to purified GST-HNF4α in vitro (Fig. 6D). However, His-Ssu72 (C12S) mutant did not bind to GST-HNF4α (Fig. 6D). The effect of phosphatase inhibitor on Ssu72 binding to HNF4α was next investigated. $Ssu72^{WT}$ primary hepatocytes transfected with HA-Ssu72 and GST-HNF4α were cultured with okadaic acid. Cells were replaced with culture media containing palmitic acid to induce hepatocyte damage. GST pull-down analyses showed that although Ssu72 and HNF4α levels were decreased in okadaic acid-treated hepatocytes, Ssu72 bound with HNF4α (Supplementary Fig. S14A). Collectively, these data indicate that Ssu72 physically binds to HNF4α.

Based on the results thus far, we hypothesized that Ssu72 may be a phosphatase of HNF4α. To examine whether HNF4α can be dephosphorylated by Ssu72, purified GST-HNF4α was phosphorylated by recombinant AMPK and incubated with purified His-Ssu72 (WT) or (C12S) mutant. GST-HNF4α was indeed dephosphorylated by His-Ssu72 (WT) but not by His-Ssu72 (C12S) mutant (Fig. 6E). Furthermore, we compared the binding affinity of Ssu72 with HNF4α WT and phosphorylation-mimicking mutants and found that the GST-HNF4α mutants interacted with Ssu72 much better than WT (Supplementary Fig. S15A, B). Taken together, these results demonstrate that Ssu72 can recognize phosphorylated HNF4α and can modify its phosphorylation levels.

Given that Ssu72-deficiency alters the phosphorylation of HNF4α, we examined its transcriptional activity after hepatic damage (Fig. 6F). As expected, HNF4α transcriptional activity in $Ssu72^{WT}$ hepatocytes was moderately decreased by hepatic damage, whereas its activity in $Ssu72^{\Delta hep}$ hepatocytes was reduced by Ssu72 deficiency (Fig. 6F). Together, our results strongly support the conclusion that Ssu72-HNF4α signaling has a critical functionality in regulating oncogenic hepatic dedifferentiation, providing novel insight into steatohepatitis-associated HCC development.

DISCUSSION

NAFLD, the most common liver disease in the world, is closely associated with hepatic insulin resistance and oxidative stress, which together represent obvious hallmarks of most metabolic diseases. NAFLD encompasses a broad spectrum of pathology from simple steatosis to NASH. It can lead to liver fibrosis, cirrhosis, and HCC. Although liver fibrosis and cirrhosis are still the main risk factors for HCC formation, emerging evidence shows that HCC can develop in earlier or later stages of NAFLD without NASH phenotype, based on similar molecular alterations found in a broad spectrum of liver diseases [1]. Our study indicates that systemic reprogramming such as hepatocyte dedifferentiation has to precede the development of NASH-associated HCC (Fig. 7). In addition, the Ssu72-deficient mouse appears to be a reliable preclinical model for genetic and functional analyses during robust NASH-to-HCC progression.

The expression of hepatic Ssu72 was decreased in patients with fatty and cirrhotic livers. However, we found that Ssu72 was also significantly downregulated in alcoholic steatohepatitis and viral hepatitis, raising the possibility that downregulation of Ssu72 could be an important molecular process for the development of HCC. Our results also indicated that enhanced immune cell infiltration and advanced NAFLD/NASH caused by Ssu72 depletion per se were not critical for HCC development. Although elderly $Ssu72^{\Delta hep}$ mice showed immune cell infiltration, inflammation, steatosis, and NASH phenotypes [15], they did not show dysplastic nodule or HCC formation without additional liver damaging stimuli. Recent studies support the notion that NASH, fibrosis, and cirrhosis per se are not sufficient for HCC development [3, 33]. These studies also suggested that the developmental progression between NASH and HCC in obesity was mechanistically separated. Therefore, typical NASH symptoms are unlikely to be the main contributors to HCC initiation. Rather, alternative mechanisms are likely to be involved. Our study strongly raises the possibility that hepatic dedifferentiation potential induced by Ssu72 depletion is a critical contributor to HCC initiation and development in response to liver injury. Several recent studies have suggested that both hepatocytes and FSC in the biliary region are capable of generating HCC [11, 12, 34, 35]. Nevertheless, it remains unclear whether hepatocyte-to-biliary cell conversion is reversible in various settings. It is also unclear how the mechanism may contribute to liver regeneration and HCC initiation. Notably, our

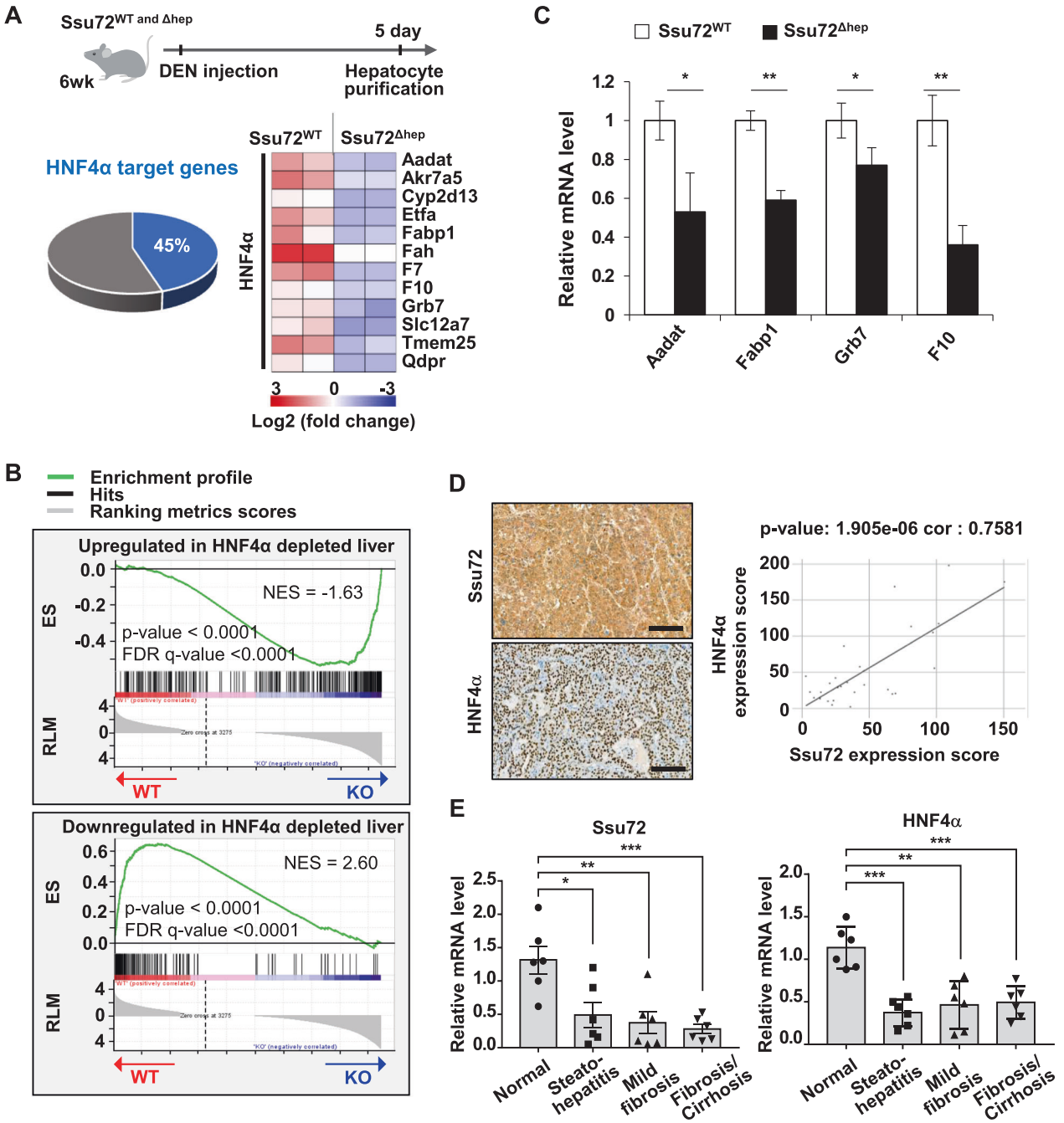

Fig. 5 Hepatic Ssu72 regulates HNF4α molecular signaling in response to liver damage. A Heat map of down- or upregulated HNF4α target genes between DEN-challenged Ssu72^{WT} and Ssu72$^{\Delta hep}$ hepatocytes. Pie charts show that among all downregulated genes, 45% are HNF4α target genes. **B** GSEA of RNA-seq data sets of DEN-challenged Ssu72^{WT} and Ssu72$^{\Delta hep}$ mice with upregulated genes in HNF4α depleted liver (top), and downregulated genes in HNF4α depleted liver (bottom) gene sets. NES normalized enrichment score, NS enrichment score, RLM ranked list metrics (Signal2Noise). **C** Relative mRNA levels of HNF4α and E2F target genes in DEN-challenged Ssu72^{WT} and Ssu72$^{\Delta hep}$ hepatocytes. Data are presented as mean ± SEM. Statistical analyses were conducted by t-test (*$p \le 0.05$ and **$p < 0.01$). **D** Representative immunohistochemical staining of NASH-associated HCC patient liver tissues (upper) (scale bar = 100 μm). Scatter plot representations show a significant correlation between Ssu72 and HNF4α expressions in HCC patient samples (bottom, $n = 31$). cor: correlation coefficient value (r). **E** Comparison of relative expression levels of Ssu72 and HNF4α mRNA in normal human specimens (no diagnostic abnormalities, $n = 10$) and specimens of patients with steatohepatitis ($n = 12$), mild fibrosis ($n = 70$), or fibrosis/cirrhosis ($n = 105$). Data are presented as mean ± SEM. Statistical analyses were conducted by two-way ANOVA (*$p \le 0.05$, **$p < 0.01$, and ***$p < 0.001$). See also Supplementary Figs. S10–12.

data demonstrated that tumor cells originated from dedifferentiated hepatocytes using genetic lineage tracing in Rosa mTmG mice. Moreover, we found that increased hepatocyte dedifferentiation in DEN and DDC-challenged Ssu72$^{\Delta hep}$ mice during NASH resulted in abnormal liver regeneration and HCC development. Therefore, Ssu72 inactivation in NASH leads to production of HCC-initiated cells by inducing hepatic dedifferentiation environments (Fig. 7). Our study also showed rare ICC development in Ssu72-deficient mice using various hepatic damage models. However, so far, the molecular mechanisms that determine HCC and ICC growth in patients and mouse models remain elusive. Recent studies have revealed that the hepatic

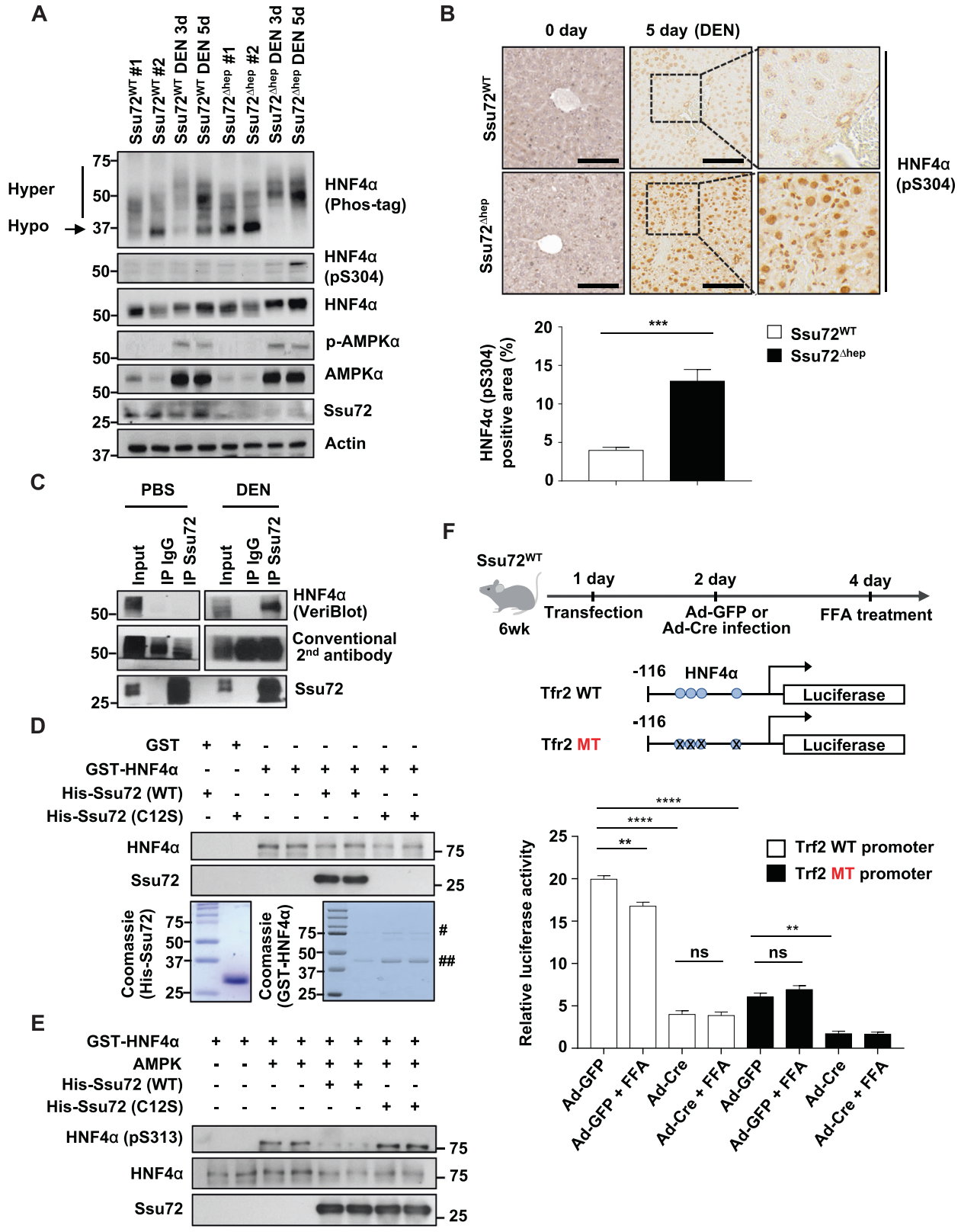

microenvironment determines lineage commitments in liver tumorigenesis [36, 37] The necroptosis-associated hepatic microenvironment predominantly induces ICC outgrowth from transformed hepatocytes, whereas HCC development is derived from the apoptotic liver microenvironment. Nevertheless, it is clear that both HCC and ICC can derive from hepatocytes. In this study, we showed that in DEN-, STAM-, or DDC-challenge Ssu72$^{\Delta hep}$ mouse models, the percentage of liver cancer due to HCC formation was ~80–90%, while the percentage of ICC and mixed HCC–ICC was 10–20%, implying that our models induce hepatic features

Fig. 6 Ssu72 negatively regulates hepatocyte oncogenic proliferation/dedifferentiation by activating HNF4α mediated transcription. A Five-week-old Ssu72^{WT} and Ssu72$^{\Delta hep}$ mice were administered with DEN (150 mg/kg) and livers from Ssu72^{WT} and Ssu72$^{\Delta hep}$ mice were harvested at 3 and 5 days. Ssu72^{WT} and Ssu72$^{\Delta hep}$ liver extracts were immunoblotted for HNF4α, AMPKα, Ssu72, and actin. Phos-tag represents a mobility shift of phosphorylated proteins using phospho-tag gel. **B** IHC staining and quantified area positive for phospho-HNF4α (pS304) in DEN-challenged Ssu72^{WT} and Ssu72$^{\Delta hep}$ livers (scale bar = 100 μm). Data are presented as mean ± SEM. Statistical analyses were conducted by t-test (***$p < 0.001$). **C** PBS or DEN treated Ssu72^{WT} and Ssu72$^{\Delta hep}$ extracts were immunoprecipitated with Ssu72 antibody. Pellets were then analyzed by immunoblotting with anti-HNF4α and anit-Ssu72 antibodies. VeriBlot secondary antibody was used to detect immunoprecipitated HNF4α without masking by IgG heavy chain. **D** Purified GST-HNF4α was incubated with purified His-Ssu72 WT or C12S mutant in vitro. #: intact form of GST-HNF4α; ##: degraded form of GST-HNF4α **E** Purified GST-HNF4α was phosphorylated by AMPK and incubated with purified His-Ssu72 WT or C12S mutant in vitro. **F** Isolated hepatocytes from Ssu72^{WT} liver were transfected with Tfr2 WT, Tfr2 mutant (MT), control, and DHFR promoter plasmids. On the 2nd day after transfection, hepatocytes were infected with control (Ad-GFP) or Cre (Ad-Cre) adenovirus. On the 4th day, hepatocytes were treated with 500 uM palmitic acid for 6 h to induce hepatocyte damage. Luciferase activity of each hepatocyte lysate was then measured. Data are presented as mean ± SEM. Statistical analyses were conducted by two-way ANOVA (**$p < 0.01$ and ****$p < 0.0001$). ChIP and qPCR analyses of HNF4α and E2F1 promoters in DEN-challenged Ssu72^{WT} and Ssu72$^{\Delta hep}$ hepatocytes. See also Supplementary Figs. S13–15.

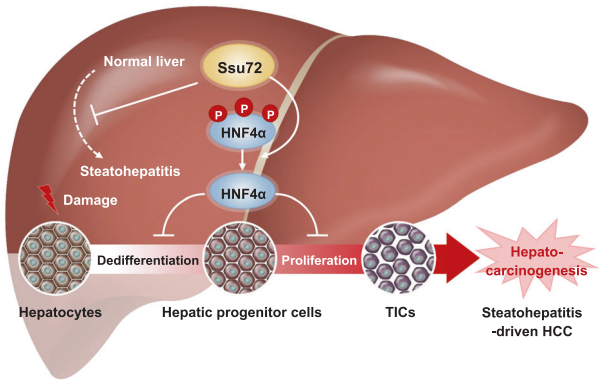

Fig. 7 Model showing how Ssu72-mediated transcriptomic signatures regulate steatohepatitis-to-HCC conversion by hepatocyte dedifferentiation. See the results and discussion sections for detailed explanation.

predominantly relevant for the HCC-associated microenvironment. Nevertheless, we believe that the administration of DEN, STAM and MCD interventions do not exclude the partial occurrence of ICC by hepatocyte dedifferentiation (Supplementary Fig. S16).

HNF4α is a transcription factor that plays a key role in hepatocyte differentiation and the maintenance of hepatic function [31]. HNF4α expression was progressively reduced during hepatocarcinogenesis [38]. In human liver tissues, HNF4α expression was also decreased in cirrhotic tissue and further decreased in hepatocarcinoma relative to healthy tissue [16]. Importantly, enforced expression of HNF4α attenuated hepatocyte epithelial–mesenchymal transition during hepatocarcinogenesis, alleviated steatohepatitis and hepatic fibrosis, and blocked HCC occurrence [38, 39], indicating that the regulation of HNF4α-mediated transcriptomics could be a promising approach for liver disease. Importantly, our data demonstrated that known or putative HNF4α target genes were remarkably downregulated in hepatocytes of DDC-challenged Ssu72$^{\Delta hep}$ mice, with concomitant increases in the levels of E2F target genes in DDC-challenged Ssu72$^{\Delta hep}$ hepatocytes. This transcriptome signature of DDC-challenged Ssu72$^{\Delta hep}$ hepatocytes also presented phenotypically and functionally as hepatic dedifferentiation. These results indicate that hepatic Ssu72 plays a key role as a driver for accurate modulation of HNF4α target genes under liver injury conditions. Our results shed light on functional mechanisms involved in tumors induced by dedifferentiation of hepatocytes rather than by biliary progenitor cell expansion during chemical-induced hepatocarcinogenesis. Our results strongly suggest that expressional regulation of hepatic Ssu72 is likely to be associated with dedifferentiation of hepatocytes during liver injury. This knowledge may improve our understanding and provide mechanistic insights into HCC progression and therapeutic treatments.

DATA AVAILABILITY

All data included in this work are presented in the paper and Supplementary Figures and Tables. Additional data relevant to this paper may be provided by the corresponding authors upon request.

REFERENCES

1. Cohen JC, Horton JD, Hobbs HH. Human fatty liver disease: old questions and new insights. Science. 2011;332:1519–23.
2. Niu ZS, Niu XJ, Wang WH. Genetic alterations in hepatocellular carcinoma: an update. World J Gastroenterol. 2016;22:9069–95.
3. Febbraio MA, Reibe S, Shalapour S, Ooi GJ, Watt MJ, Karin M. Preclinical models for studying NASH-driven HCC: how useful are they? Cell Metab. 2019;29:18–26.
4. Severi T, van Malenstein H, Verslype C, van Pelt JF. Tumor initiation and progression in hepatocellular carcinoma: risk factors, classification, and therapeutic targets. Acta Pharmacol Sin. 2010;31:1409–20.
5. Gaudio E, Carpino G, Cardinale V, Franchitto A, Onori P, Alvaro D. New insights into liver stem cells. Digestive Liver Dis. 2009;41:455–62.
6. Kitade M, Kaji K, Yoshiji H. Relationship between hepatic progenitor cell-mediated liver regeneration and non-parenchymal cells. Hepatol Res. 2016;46:1187–93.
7. Tarlow BD, Pelz C, Naugler WE, Wakefield L, Wilson EM, Finegold MJ, et al. Bipotential adult liver progenitors are derived from chronically injured mature hepatocytes. Cell Stem Cell. 2014;15:605–18.
8. He GB, Dhar D, Nakagawa H, Font-Burgada J, Ogata H, Jiang YH, et al. Identification of liver cancer progenitors whose malignant progression depends on autocrine IL-6 signaling. Cell. 2013;155:384–96.
9. Font-Burgada J, Shalapour S, Ramaswamy S, Hsueh B, Rossell D, Umemura A, et al. Hybrid periportal hepatocytes regenerate the injured liver without giving rise to cancer. Cell. 2015;162:766–79.
10. Miyaoka Y, Miyajima A. To divide or not to divide: revisiting liver regeneration. Cell Div. 2013;8:8.
11. Fan B, Malato Y, Calvisi DF, Naqvi S, Razumilava N, Ribback S, et al. Cholangiocarcinomas can originate from hepatocytes in mice. J Clin Investig. 2012;122:2911–5.
12. Sekiya S, Suzuki A. Intrahepatic cholangiocarcinoma can arise from Notch-mediated conversion of hepatocytes. J Clin Investig. 2012;122:3914–8.
13. Kim HS, Baek KH, Ha GH, Lee JC, Kim YN, Lee J, et al. The hsSsu72 phosphatase is a cohesin-binding protein that regulates the resolution of sister chromatid arm cohesion. Embo J. 2010;29:3544–57.
14. Kim HS, Kim SH, Park HY, Lee J, Yoon JH, Choi S, et al. Functional interplay between Aurora B kinase and Ssu72 phosphatase regulates sister chromatid cohesion. Nat Commun. 2013;4:2631.
15. Kim SH, Jeon Y, Kim HS, Lee JK, Lim HJ, Kang D, et al. Hepatocyte homeostasis for chromosome ploidization and liver function is regulated by Ssu72 protein phosphatase. Hepatology. 2016;63:247–59.
16. Subramanian A, Tamayo P, Mootha VK, Mukherjee S, Ebert BL, Gillette MA, et al. Gene set enrichment analysis: A knowledge-based approach for interpreting genome-wide expression profiles. Proc Natl Acad Sci USA. 2005;102:15545–50.
17. Aizarani N, Saviano A, Sagar, Mailly L, Durand S, Herman JS, et al. A human liver cell atlas reveals heterogeneity and epithelial progenitors. Nature. 2019;572:199–204.
18. Lim E, Wu D, Pal B, Bouras T, Asselin-Labat ML, Vaillant F, et al. Transcriptome analyses of mouse and human mammary cell subpopulations reveal multiple conserved genes and pathways. Breast Cancer Res. 2010;12:1–14.
19. Walesky C, Edwards G, Borude P, Gunewardena S, O'Neil M, Yoo B, et al. Hepatocyte nuclear factor 4 alpha deletion promotes diethylnitrosamine-induced hepatocellular carcinoma in rodents. Hepatology. 2013;57:2480–90.

20. Sun K, Montana V, Chellappa K, Brelivet Y, Moras D, Maeda Y, et al. Phosphorylation of a conserved serine in the deoxyribonucleic acid binding domain of nuclear receptors alters intracellular localization. Mol Endocrinol. 2007;21:1297–311.
21. Vető B, Bojcsuk D, Bacquet C, Kiss J, Sipeki S, Martin L, et al. The transcriptional activity of hepatocyte nuclear factor 4 alpha is inhibited via phosphorylation by ERK1/2. PLoS ONE. 2017;12:e0172020.
22. Guo HT, Gao CJ, Mi ZY, Wai PY, Kuo PC. Phosphorylation of Ser(158) regulates inflammatory redox-dependent hepatocyte nuclear factor-4 alpha transcriptional activity (Retracted article. See vol. 461, pg. 347, 2014). Biochem J. 2006;394:379–87.
23. Chellappa K, Jankova L, Schnabl JM, Pan SQ, Brelivet Y, Fung CLS, et al. Src tyrosine kinase phosphorylation of nuclear receptor HNF4 alpha correlates with isoform-specific loss of HNF4 alpha in human colon cancer. Proc Natl Acad Sci USA. 2012;109:2302–7.
24. Wang ZY, Salih E, Burke PA. Quantitative analysis of cytokine-induced hepatocyte nuclear factor-4 alpha phosphorylation by mass spectrometry. Biochemistry. 2011;50:5292–300.
25. Fujii M, Shibazaki Y, Wakamatsu K, Honda Y, Kawauchi Y, Suzuki K, et al. A murine model for non-alcoholic steatohepatitis showing evidence of association between diabetes and hepatocellular carcinoma. Med Mol Morphol. 2013;46:141–52.
26. Kang JS, Wanibuchi H, Morimura K, Gonzalez FJ, Fukushima S. Role of CYP2E1 in diethylnitrosamine-induced hepatocarcinogenesis in vivo. Cancer Res. 2007;67:11141–6.
27. Halpern KB, Shenhav R, Matcovitch-Natan O, Toth B, Lemze D, Golan M, et al. Single-cell spatial reconstruction reveals global division of labour in the mammalian liver. Nature. 2017;542:352–6.
28. Miyajima A, Tanaka M, Itoh T. Stem/progenitor cells in liver development, homeostasis, regeneration, and reprogramming. Cell Stem Cell. 2014;14:561–74.
29. Tatetsu H, Kong NR, Chong G, Amabile G, Tenen DG, Chai L. SALL4, the missing link between stem cells, development and cancer. Gene. 2016;584:111–9.
30. Oikawa T, Kamiya A, Kakinuma S, Zeniya M, Nishinakamura R, Tajiri H, et al. Sall4 Regulates Cell Fate Decision in Fetal Hepatic Stem/Progenitor Cells. Gastroenterology. 2009;136:1000–11.
31. Lu H. Crosstalk of HNF4α with extracellular and intracellular signaling pathways in the regulation of hepatic metabolism of drugs and lipids. Acta Pharm Sin B. 2016;6:393–408.
32. Yeh MM, Bosch DE, Daoud SS. Role of hepatocyte nuclear factor 4-alpha in gastrointestinal and liver diseases. World J Gastroenterol. 2019;25:4074–91.
33. Grohmann M, Wiede F, Dodd GT, Gurzov EN, Ooi GJ, Butt T, et al. Obesity Drives STAT-1-Dependent NASH and STAT-3-Dependent HCC. Cell. 2018;175:1289–306.e20.
34. Guest RV, Boulter L, Kendall TJ, Minnis-Lyons SE, Walker R, Wigmore SJ, et al. Cell lineage tracing reveals a biliary origin of intrahepatic cholangiocarcinoma. Cancer Res. 2014;74:1005–10.
35. Mu X, Español-Suñer R, Mederacke I, Affò S, Manco R, Sempoux C, et al. Hepatocellular carcinoma originates from hepatocytes and not from the progenitor/biliary compartment. J Clin Investig. 2015;125:3891–903.
36. Seehawer M, Heinzmann F, D'Artista L, Harbig J, Roux PF, Hoenicke L, et al. Necroptosis microenvironment directs lineage commitment in liver cancer. Nature. 2018;562:69–75.
37. Bellanti F, di Bello G, Iannelli G, Pannone G, Pedicillo MC, Boulter L, et al. Inhibition of nuclear factor (erythroid-derived 2)-like 2 promotes hepatic progenitor cell activation and differentiation. Npj Regen Med. 2021;6:1–12.
38. Ning BF, Ding J, Yin C, Zhong W, Wu K, Zeng X, et al. Hepatocyte nuclear factor 4 alpha suppresses the development of hepatocellular carcinoma. Cancer Res. 2010;70:7640–51.
39. Yin C, Lin Y, Zhang X, Chen YX, Zeng X, Yue HY, et al. Differentiation therapy of hepatocellular carcinoma in mice with recombinant adenovirus carrying hepatocyte nuclear factor-4alpha gene. Hepatology. 2008;48:1528–39.

ACKNOWLEDGEMENTS

We would like to thank Dr. Valentina Factor (National Cancer institute, Bethesda, MD) and Dr. Shunsuke Matsuo (Gunma University, Japan) for kindly providing A6 antibody and Tfr2 promoter constructs, respectively.

AUTHOR CONTRIBUTIONS

HSK and JSY designed the studies, performed and analyzed data, and wrote the parts of paper; YJ and HL generated conditional KO mice and analyzed data; EJP, JKL, SC, JYP, and HG contributed to specific experiments; CWL designed the studies, supervised the overall project, wrote the paper, and performed the final paper preparation. All authors provided feedback and agreed on the final paper.

FUNDING

This work was supported by grants [2017R1A2B3006776 (CWL) and 2018R1D1A1A02085616 (HSK)] of National Research Foundation (NSF) funded by the Ministry of Education, Science, and Technology (MEST), Republic of Korea.

COMPETING INTERESTS

The authors declare no competing interests.

ETHICS APPROVAL

All animal experiments were conducted in accordance with guidelines of the IACUC 2018-05-16-2, IACUC 2019-04-31-1, IACUC 2020-08-33-1 and IACUC 2021-02-41-1 of Sungkyunkwan University, an institution accredited by the Association for Assessment and Accreditation of Laboratory Animal Care International. Research with human liver specimens was approved by the Asan Medical Center Institutional Review Board (2019-0636).

ADDITIONAL INFORMATION

Supplementary information The online version contains supplementary material available at https://doi.org/10.1038/s41418-021-00877-x.

Correspondence and requests for materials should be addressed to Hyun-Soo Kim or Chang-Woo Lee.